Characterization of Non-Wide-Sense Stationarity for Distributed Massive MIMO Channels

Xu, Yingjie; Sandra, Michiel; Cai, Xuesong; Willhammar, Sara; Tufvesson, Fredrik

Published in:
19th European Conference on Antennas and Propagation (EuCAP) 2025

2024

Document Version:
Peer reviewed version (aka post-print)

Characterization of Non-Wide-Sense Stationarity for Distributed Massive MIMO Channels

Yingjie Xu*, Michiel Sandra*, Xuesong Cai*† Sara Willhammar* Fredrik Tufvesson*
*Department of Electrical and Information Technology, Lund University, Lund, Sweden
†School of Electronics, Peking University, Beijing, China
E-mail: {yingjie.xu, michiel.sandra, xuesong.cai, sara.willhammar, fredrik.tufvesson}@eit.lth.se, xuesong.cai@pku.edu.cn

***Abstract*—Distributed massive multiple-input multiple-output (MIMO) communication is envisioned as one of the key paradigms of future MIMO systems. To investigate non-wide-sense stationarities (non-WSSs) in distributed massive MIMO channels, this paper first presents an indoor channel measurement campaign, where distributed arrays with a total of 128 elements were implemented. Then relying on the correlation matrix distance (CMD) method, the stationary distance and stationary frequency of the measured channels are estimated. Results show that the space non-WSS in the measured channels is significantly affected by locations of the distributed arrays. However, the impact of array locations on the measured frequency non-WSSs is marginal. Besides, even for a specific channel, the estimated stationary distances at the base station (BS) and user equipment (UE) side are different. The results provide insights from the perspective of channel non-WSS for future modelling of distributed massive MIMO channels and deployment of distributed antennas in practical systems.**

***Index Terms*—6G wireless communication, distributed massive MIMO, channel measurements, channel non-wide-sense stationarity.**

I. Introduction

Distributed massive multiple-input multiple-output (MIMO) communication, also known as cell-free massive MIMO [1], is viewed as a promising technology for sixth-generation (6G) wireless communication networks. With this technology, individual or grouped antennas are distributed over a large geographical area, featuring both large-scale antenna gain and spatial multiplexing gain [2], [3]. Research on propagation channels in distributed massive MIMO systems is ongoing. One important channel characteristic is channel wide-sense stationarity (WSS), which means that the channel's statistical properties remain unchanged in a certain domain, e.g., time/space/frequency [4]. Correspondingly, the maximum intervals in the time/space/frequency domain, where channels are viewed as wide-sense stationary, are defined as stationary time/distance/frequency.

The assumption of the channel being wide-sense stationary may not hold in distributed massive MIMO systems. On the one hand, in the space domain, the deployment of large-scale antenna systems results in multipath components (MPCs) being visible for only parts of the antennas while being invisible to others. This leads to varying channel statistics over the antennas, which is referred to as space non-WSS. Several studies have demonstrated that space non-WSS in massive MIMO channels is prominent. Large power variations were observed over the large-scale array in channel measurements reported in [5]. Then, to model space non-WSS channels, the concept of 'visibility regions' for the large array was proposed in [6]. The behaviors of channel non-WSS in a large-scale uniform linear array were studied in [7]. However, these studies are mainly focusing on channels with co-located massive MIMO arrays. In distributed massive MIMO channels, the distributed access points (APs) at the base station (BS) end and the movement of the user equipment (UE) will further make the channels spatially variable. The related space non-WSS behavior needs to be investigated.

Furthermore, when a wide communication bandwidth is implemented in a system, the transmission coefficients of a signal vary over the different frequency components [8]. This leads to frequency-varying channel statistics and results in frequency non-WSS in the channels. The study in [9] found that the K-factor varies with frequency in the measured vehicular channels. A frequency-dependent path gain and correlations between scatterers were introduced in [10] and [11] for characterizing frequency non-WSS in channels. Note that these studies only consider single-link MIMO channels. There is still a gap in the literature about frequency non-WSS characterization of multi-link channels, which is one of the key features of distributed massive MIMO channels.

To the best of our knowledge, the characterization of non-WSS in distributed massive MIMO channels, here also strengthened by using actual measurement data, has not been fully explored in the literature. To fill this gap, a multi-link distributed massive MIMO channel measurement campaign is presented here. Then the space-time-frequency correlation matrix distance (CMD) is introduced as a measure of channel non-WSS. Finally, the multi-link space and frequency non-WSS behavior in measured channels is investigated, and the impact of antenna location on channel non-WSSs is evaluated.

The remainder of this paper is organized as follows. Section II introduces the environment and setup for the channel measurements. Then, Section III presents the CMD-based method for evaluating channel non-WSS. Section IV outlines the characterization of channel non-WSSs based on measurement data. Finally, conclusions are drawn in Section V.

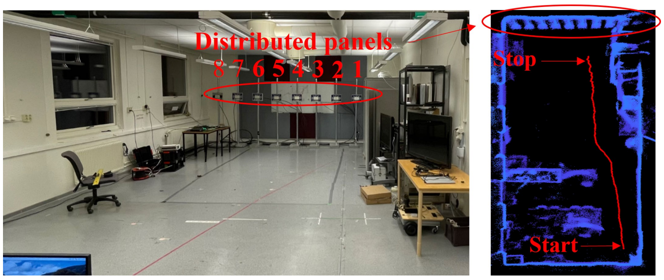

Fig. 1. Photo of the measurement environment (left) and top-view geometry with the UE trajectory based on LIDAR output (right).

II. Measurement Environment and Setup

The measurement campaign was performed in an indoor lab room, as depicted in Fig. 1. The room dimensions are approximately $15\times6\times2.5$ m^3. There are numerous objects in the room, e.g., desks, chairs, steel storage cabinets, and screens, which contribute to various reflections, scattering, diffraction, and blocking behaviors of the signal propagating. The measurements were performed at a carrier frequency of 5.7 GHz with 400 MHz bandwidth. A wideband USRP-based distributed massive MIMO channel sounder [12] was used for collecting the channel data. A total of eight uniform planar arrays were deployed at the BS end. They are here referred to as 'panels', and are evenly distributed along one side of the room, as shown in Fig. 1. The space between the adjunct panels is approximately 60 cm. Each panel was implemented with 2×4 dual-polarized patch elements (16 ports in total). At the UE end, a single monopole antenna was fixed on a robot that can move via remote control. Before the measurements, back-to-back calibration was performed to eliminate responses from the sounding system, connectors, and cables. For system synchronization, two GPS-disciplined Rubidium (Rb) clocks were deployed at the BS and UE ends, respectively. The sounding signal, a 1024-length Zadoff-Chu sequence, was transmitted from the monopole antenna. During the measurements, the robot moved from one end of the room toward the panels with a constant speed of 0.012 m/s. Its trajectory and exact positions were recorded by a LIDAR sensor. In total, the channel links from all panels were measured along an approximately 12-meter-long route, as shown in Fig. 1, with 128×1017 snapshots collected.

III. Metric of Channel Non-WSS Stationarities

The channel space/frequency WSS is referred to as a finite region in the space/frequency domain in which channel statistic properties are considered unchanged [4]. Several methods have been widely used for evaluating WSSs of channels, including CMD, average power density profile (APDP)-based, spectral divergence (SD), and shadow fading correlation-based metrics. Among them, the CMD method is able to show detailed information of channel WSSs at both the BS and UE side [13]. It is implemented by analyzing similarities between channel correlation matrices along the space or frequency axis. If the similarity level is above a specific threshold, then the channel within that span of space or frequency can be viewed as statistically wide-sense stationary. The time-space-frequency correlation matrix of the channels from the p-th antenna array at time instant t_i and frequency f_m is defined as

$$\mathbf{R}(p,t_i,f_m) = \frac{1}{W\cdot L}\sum_{f=f_m-W/2}^{f_m+W/2}\sum_{t=t_i}^{t_i+L-1}\mathbf{h}_p(t,f)\mathbf{h}_p(t,f)^{\mathrm{H}} \tag{1}$$

where L and W are the lengths of the sliding windows in the space and frequency domain, respectively. Note that the sliding windows should be large enough to accurately estimate correlation matrices but also small enough that within these intervals the channel's statistical behaviors can be viewed as unchanged [13]. Here, the lengths are determined based on the coherence distance D_c and the coherence bandwidth B_c of the channels since these are space and frequency intervals, respectively, in which channels can be considered as unchanged. Given a constant speed v_{UE} of the UE, the intervals can be obtained as the minimum space and frequency intervals that fulfill the condition when the channel's auto-correlation function (ACF) $\sigma(\Delta d)$ and frequency correlation function (FCF) $\Lambda(\Delta f)$ decrease to specific thresholds c_{th}^D and c_{th}^F [14], [15], respectively, i.e.,

$$D_c = \min\{\Delta d > 0 : \sigma(\Delta d) = c_{th}^D\} \tag{2}$$

$$B_c = \min\{\Delta f > 0 : \Lambda(\Delta f) = c_{th}^F\} \tag{3}$$

where the ACF is expressed as

$$\sigma(\Delta d) = \mathbf{E}\{\frac{\mathbf{H}(t,f)\mathbf{H}(t+\Delta d/v_{UE},f)^{\mathrm{H}}}{\|\mathbf{H}(t,f)\|_{\mathrm{F}}\|\mathbf{H}(t+\Delta d/v_{UE},f)\|_{\mathrm{F}}}\} \tag{4}$$

and the FCF is given by

$$\Lambda(\Delta f) = \mathbf{E}\{\frac{\mathbf{H}(t,f)\mathbf{H}(t,f+\Delta f)^{\mathrm{H}}}{\|\mathbf{H}(t,f)\|_{\mathrm{F}}\|\mathbf{H}(t,f+\Delta f)\|_{\mathrm{F}}}\}. \tag{5}$$

Then, based on (1), the space-time-frequency CMD between two distributed arrays, p and q, the time instants t_i and t_j, and frequencies f_m and f_n is defined as

$$d(p,q;t_i,t_j;f_m,f_n) = 1 - \frac{\mathrm{tr}\{\mathbf{R}(p,t_i,f_m)\cdot\mathbf{R}(q,t_j,f_n)\}}{\|\mathbf{R}(p,t_i,f_m)\|_{\mathrm{F}}\|\mathbf{R}(q,t_j,f_n)\|_{\mathrm{F}}}. \tag{6}$$

By setting arrays $p=q$ and time instants $t_i=t_j$, (6) is reduced to the CMD $d_F(p,t_i,f_m,f_n)$ in the frequency domain. Then the stationary frequency B_s is given as the maximum frequency difference over which $d_F(p,t_i,f_m,f_n)$ remains below a certain threshold d_{th}^F, and is expressed as

$$B_s(p,t_i,f_m) = f_{\max} - f_{\min} \tag{7}$$

where

$$\begin{cases} f_{\min} = \arg\max\limits_{f_c-B/2\le f_n<f_m} d_F(p,t_i,f_m,f_n) \ge d_{th}^F \\ f_{\max} = \arg\min\limits_{f_m\le f_n\le f_c+B/2} d_F(p,t_i,f_m,f_n) \ge d_{th}^F \end{cases} \tag{8}$$

with carrier frequency and bandwidth denoted as f_c and B, respectively. Similarly, to investigate the spatial evolution at both BS and UE sides, the CMD $d_S^{BS}(p,q,t_i,f_m)$ and $d_S^{UE}(p,t_i,t_j,f_m)$ can be obtained from (6) by setting $t_i=t_j, f_m=f_n$ and $p=q, f_n=f_m$, respectively. Then the stationary distance $D_s^{BS}(p,q,t_i,f_m)$ at the BS side is given by

$$D_s^{BS}(p,q,t_i,f_m)=(p_{\max}-p_{\min})\cdot\Delta d \tag{9}$$

where Δd represents the space between the distributed arrays, and

$$\begin{cases} p_{\min}=\arg\max\limits_{1\leq q<p} d_S^{BS}(p,q,t_i,f_m)\geq d_{th}^{BS} \\ p_{\max}=\arg\min\limits_{p\leq q\leq M_T} d_S^{BS}(p,q,t_i,f_m)\geq d_{th}^{BS} \end{cases} \tag{10}$$

with the total number of distributed arrays denoted as M_T. The stationary distance $D_S^{UE}(p,t_i,t_j,f_m)$ at the UE side is given by

$$D_s^{UE}(p,t_i,f_m)=(t_{\max}-t_{\min})\cdot v_{UE} \tag{11}$$

where

$$\begin{cases} t_{\min}=\arg\max\limits_{0\leq t_j<t_i} d_S^{UE}(p,f_m,t_i,t_j)\geq d_{th}^{UE} \\ t_{\max}=\arg\min\limits_{t_i\leq t_j\leq t_{\max}} d_S^{UE}(p,f_m,t_i,t_j)\geq d_{th}^{UE} \end{cases}. \tag{12}$$

The results of B_s, D_s^{BS} and D_s^{UE} are related with the thresholds d_{th}^{F}, d_{th}^{BS}, and d_{th}^{UE}, respectively. The less restrictive the threshold is, the larger the stationary distance/frequency is. In this paper, a suitable threshold value $d_{th}^{F}=d_{th}^{BS}=d_{th}^{UE}=0.2$ is considered, as recommended in [13].

IV. Measurement Results and Analysis

A. Sliding window

As mentioned, the sliding window length in (1) is determined by evaluating the coherence time and coherence bandwidth of the channels. Figs. 2a and 2b illustrate the absolute values of the ACF and FCF of the measured channels, respectively. Different ACF and FCF behaviors are observed during the movement of the UE and from different panels, meaning that the second-order channel statistics vary spatially, and are further indicating that the channels are space non-wide-sense stationary. To determine D_c and B_c, the thresholds c_{th}^{D} and c_{th}^{F} in (2) and (3) are both set to 0.5, as suggested in [14]. For instance, the channel ACF and FCF of panel 1 at $t=200$ s drop below 0.5 when $\Delta d=0.13$ m and $\Delta f=12$ MHz, which are then viewed as the corresponding coherence distance and bandwidth, respectively. The channel ACFs and FCFs are measured at each time instant and in each panel, and the coherence distance D_c and the coherence bandwidth B_c are evaluated using (2) and (3), respectively, which are summarized in Table I. According to the results, the lengths L and W of the sliding window in the space and frequency domains are set to be less than the mean values of D_c and B_c, i.e., 0.1 m and 20 MHz, respectively.

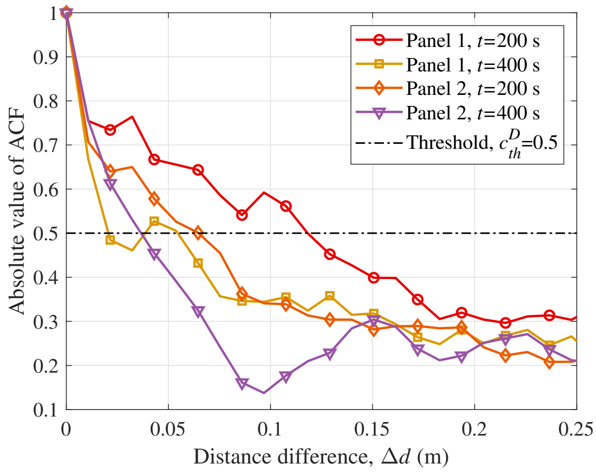

(a)

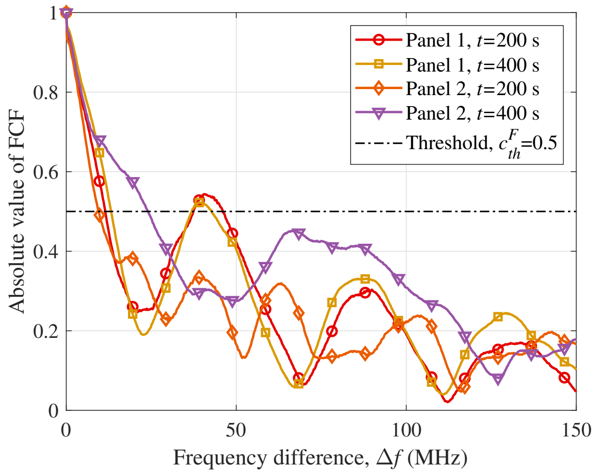

(b)

Fig. 2. The absolute values of the ACF (a) and FCF (b) of the measured channels from panel 1 and 2 at $t=200$ and 400 s.

B. Space-frequency non-WSS

Based on the space-time-frequency CMD metric presented in Section III, the space and frequency non-WSS of the measured distributed massive MIMO channels are evaluated. Firstly, the box chart of the measured channel stationary distance D_s^{UE} at the UE end is shown in Fig. 3. The chart consists of the maximum, minimum, 75% percentile, 25% percentile, median, and average values of the measured D_s^{UE}. It is found that the channels from panel 4 exhibit the largest maximum and 75% percentile values of D_s^{UE}, while channels from panel 5 show the largest average values. The smallest minimum and average values are observed in channels from panel 1 and 2, respectively. There is a trend that the channels of the side panels (i.e., panel 1, 2, 7, and 8) tend to exhibit smaller D_s^{UE} than those of the middle panels (i.e., panel 4 and 5). This is reasonable since the panels on the sides are closer to the sidewalls of the room, making them more likely to receive

TABLE I
COHERENCE TIME AND COHERENCE BANDWIDTH AS MEASURED FROM DIFFERENT PANELS.

Panel	Coherence distance, D_c (m)	Coherence bandwidth, B_c (MHz)
1	0.14	23.8
2	0.13	25.3
3	0.12	24.1
4	0.13	27.6
5	0.11	22.2
6	0.12	22.2
7	0.11	19.5
8	0.17	35.9
Mean	0.13	25.1

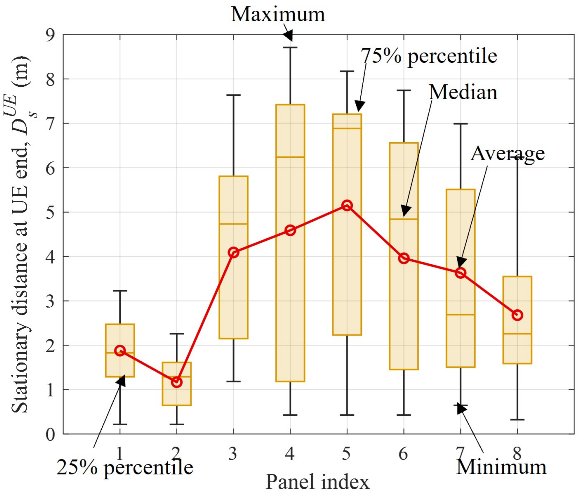

Fig. 3. Box chart of channel stationary distance D_s^{UE} as measured from different panels.

those MPCs reflected or scattered from the walls. Compared to the dominant line-of-sight (LoS) path, these MPCs are less stable. They may appear and disappear more frequently during the movement of the UE, resulting in a shorter stationary distance at the UE end.

Fig. 4 illustrates the comparisons of the stationary distance D_s^{BS} at the BS end as measured from different panels. For the same panel, the stationary distance changes with time. This means that during the movement of the UE, due to the rich scattering environment in the measured room, the MPCs with varying levels of 'stability' appear and disappear in the channels, thus contributing to a dynamic non-stationarity of channels. For instance, for the channels from panel 5, the largest stationary distance $D_s^{BS} = 3.42$ m is found when $t = 600$ s, while the smallest one with 1.14 m is observed at $t = 200$ s. Furthermore, compared to those of the panels near the sidewalls, the channels of the middle panels tend to exhibit larger D_s^{BS}. These results are consistent with those

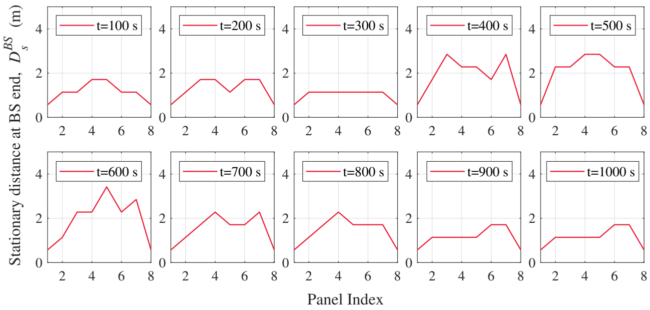

Fig. 4. Comparisons of stationary distance D_s^{BS} as measured from different panels.

found in D_s^{UE}, indicating that in the measured environments, the locations of the distributed panels have a significant impact on channel space non-WSS. The mean, standard deviation, and minimum values of B_c^{UE} and B_c^{BS} measured from different panels are summarized in TABLE II. Note that even for channels from a specific panel, the stationary distances B_c^{UE} and B_c^{BS} are different, which provides insights into future modeling of distributed massive MIMO channels.

The stationary frequency B_s^F as measured during the movement of the UE is depicted in Fig. 5. For a specific panel, it can be found that a larger stationary frequency is generally observed when the UE is further from the starting point, i.e., closer to the panels. Moreover, a stationary frequency over 350 MHz is measured in several panels when the UE is extremely close to them. At this time, the measured channels can be viewed as frequency wide-sense stationary over almost the whole measured bandwidth. Compared to the environment, we conjecture that this is because when the UE moves towards the panels, the LoS component becomes stronger and more dominant. Since it is much more stable compared to other weaker reflected or scattered MPCs, it results in larger stationary intervals in the frequency domain. Furthermore, the cumulative distribution functions (CDFs) of the measured B_s^F from different panels are shown in Fig. 6. Unlike the results of stationary distance, the locations of the distributed panels do not exhibit a strong impact on the stationary frequency in the measured environment. The mean, standard deviation, and minimum values of B_c^F measured from different panels are also summarized in TABLE II.

V. CONCLUSIONS

In this paper, an indoor distributed massive MIMO channel measurement campaign has been performed. Based on the measurement data, the channel space and frequency non-WSS have been investigated. The channel stationary distance and stationary frequency have been extracted via the space-time-frequency CMD method. From the results, different space non-WSSs have been observed from different distributed antennas. Channels from those antennas near the sidewalls of the room are more likely to exhibit smaller stationary distances, resulting in more significant space non-WSS. However, for channel frequency non-WSS, marginal differences have been

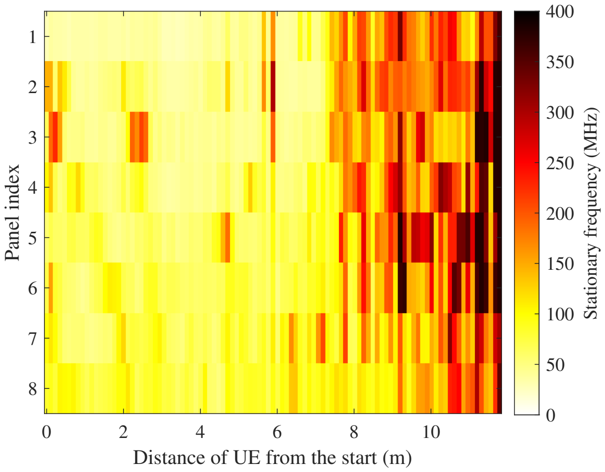

Fig. 5. Comparisons of measured stationary frequency during the movement of the UE.

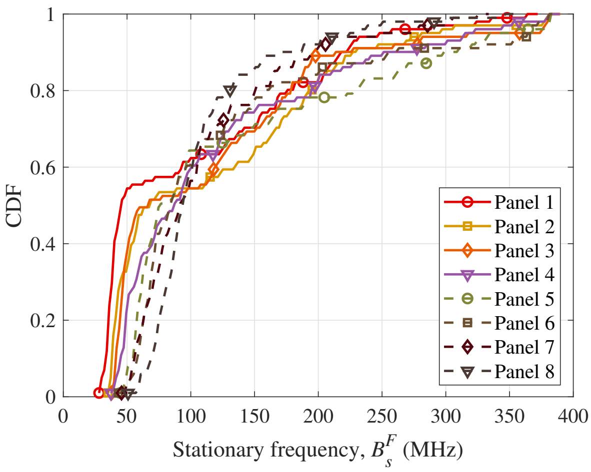

Fig. 6. CDFs of the measured stationary frequency from different panels.

observed in the channels from different panels. These findings will provide insights to the practical antenna deployment in future distributed massive MIMO systems from the channel non-stationarity perspective. In addition, different stationary distances have been observed at the BS and UE ends for specific measured channels, contributing to insights into future modeling of distribute massive MIMO channels.

ACKNOWLEDGMENT

This work was supported by the Swedish strategic research area ELLIIT and by REINDEER, which has received funding from the European Union's Horizon 2020 research and innovation program under grant agreement No. 101013425.

TABLE II
STATIONARY DISTANCE AND FREQUENCY OF THE MEASURED CHANNELS.

	D_s^{UE} (m)			D_s^{BS} (m)			B_s^F (MHz)		
Panel	Mean	Std.	Min.	Mean	Std.	Min.	Mean	Std.	Min.
1	1.9	0.8	0.2	0.6	0.1	0.6	100.1	83.5	28.1
2	1.2	0.6	0.2	1.3	0.4	1.1	117.1	89.0	35.2
3	4.1	1.8	1.2	1.8	0.5	1.1	114.3	90.1	37.9
4	4.6	2.9	0.4	2.0	0.6	1.1	130.0	98.9	44.7
5	5.2	2.7	0.4	2.1	0.9	1.1	130.0	98.9	44.7
6	4.0	2.5	0.4	1.8	0.5	1.1	110.9	61.7	45.7
7	3.6	2.2	0.6	2.1	0.7	1.1	110.9	61.7	45.7
8	2.7	1.6	0.3	0.6	0.1	0.6	109.0	51.0	50.8

REFERENCES

[1] H. Q. Ngo, A. Ashikhmin, H. Yang, E. G. Larsson, and T. L. Marzetta, "Cell-free massive MIMO versus small cells," *IEEE Trans. Wireless Commun.*, vol. 16, no. 3, pp. 1834–1850, Mar. 2017.

[2] Z. Chen and E. Björnson, "Channel hardening and favorable propagation in cell-free massive MIMO with stochastic geometry," *IEEE Trans. Commun.*, vol. 66, no. 11, pp. 5205–5219, Nov. 2018.

[3] Y. Xu, M. Sandra, X. Cai, S. Willhammar, F. Tufvesson, "Spatial seperation of closely-spaced users in measured distributed massive MIMO channels," in *Proc. IEEE SPAWC'24*, Lucca, Italy, 2024, pp. 1–6.

[4] G. Matz, "On non-WSSUS wireless fading channels" *IEEE Trans. Wireless Commun.*, vol. 4, no. 5, pp. 2465–2478, Sep. 2005.

[5] X. Gao, O. Edfors, F. Tufvesson, and E. G. Larsson, "Massive MIMO in real propagation environments: Do all antennas contribute equally?" *IEEE Trans. Commun.*, vol. 63, no. 11, pp. 3917–3928, Nov. 2015.

[6] J. Flordelis, X. Li, O. Edfors, and F. Tufvesson, "Massive MIMO extensions to the COST 2100 channel model: Modeling and validation," *IEEE Trans. Wireless Commun.*, vol. 19, no. 1, pp. 380–394, Jan. 2020.

[7] W. Zuo *et al.*, "Analysis of spatial non-stationary characteristics for 6G XL-MIMO communication," in *Proc. IEEE VTC'24-Spring*, Singapore, 2024, pp. 1–6.

[8] X. Cheng, Z. Huang, and L. Bai, "Channel nonstationarity and consistency for beyond 5G and 6G: A survey," *IEEE Commun. Surveys Tuts.*, vol. 24, no. 3, pp. 1634–1669, 3rd Quart., 2022.

[9] L. Bernado, T. Zemen, F. Tufvesson, A. F. Molisch, and C. F. Mecklenbräuker, "Time- and frequency-varying k-factor of non-stationary vehicular channels for safety-relevant scenarios," *IEEE Trans. Intell. Transp. Syst.*, vol. 16, no. 2, pp. 1007–1017, Apr. 2015.

[10] Z. Huang, X. Cheng, and X. Yin, "A general 3D non–stationary 6G channel model with time-space consistency," *IEEE Trans. Commun.*, vol. 70, no. 5, pp. 3436–3450, May 2022.

[11] Z. Huang and X. Cheng, "A general 3D space–time–frequency nonstationary model for 6G channels," *IEEE Trans. Wireless Commun.*, vol. 20, no. 1, pp. 535–548, Jan. 2021.

[12] M. Sandra, C. Nelson, X. Li, X. Cai, F. Tufvesson, and A. J. Johansson, "A wideband distributed massive MIMO channel sounder for communication and sensing", *IEEE Trans. Antennas Propag.*, submitted for publication. https://arxiv.org/abs/2403.11856.

[13] R. He et al., "Characterization of quasi-stationarity regions for vehicleto-vehicle radio channels," *IEEE Trans. Antennas Propag.*, vol. 63, no. 5, pp. 2237–2251, May 2015.

[14] C.-X. Wang, Z. Lv, Y. Chen, and H. Haas, "A complete study of space-time-frequency statistical properties of the 6G pervasive channel model," *IEEE Trans. Commun.*, vol. 71, no. 12, pp. 7273–7287, Dec. 2023.

[15] Y. Xu, K. Yu, L. Li, X. Lei, L. Hao, and C.-X. Wang, "A 3D non-stationary mmWave channel model for vacuum tube ultra-high-speed train wireless communication systems," in *Proc. IEEE WCNC'21*, Nanjing, China, 2021, pp. 1–6.

[16] D. W. Matolak, "Channel modeling for vehicle-to-vehicle communications," *IEEE Commun. Mag.*, vol. 46, no. 5, pp. 76–83, May 2008.